MDPI

Article

The Influence of Hydrothermal Temperature on Alumina Hydrate and Ammonioalunite Synthesis by Reaction Crystallization

Junkai Wang, Laishi Li *, Yusheng Wu * and Yuzheng Wang

School of Material Science and Engineering, Shenyang University of Technology, Shenyang 110870, China
* Correspondence: lilaishi@sut.edu.cn (L.L.); wuyus@sut.edu.cn (Y.W.)

Abstract: With the rapid development of the alumina industry and the shortage of bauxite, high-alumina coal fly ash (HACFA) has attracted more and more attention as a potential alternative alumina resource. In order to extract alumina from HACFA with newly developed technology, the investigation of the crucial step, the reaction between $NH_4Al(SO_4)_2 \cdot 12H_2O$ and $NH_3 \cdot H_2O$, is necessary and valuable. Thermodynamic analyses have shown that four kinds of alumina hydrate (boehmite, diaspore, gibbsite, and bayerite) might be formed at 120–200 °C, and ammonioalunite might be formed at temperatures over 180 °C. A hydrothermal reaction crystallization method was applied to this reaction. The experimental results showed that boehmite (AlOOH) could be formed at 150 °C and 200 °C after 12 h and $NH_4Al_3(SO_4)_2(OH)_6$, an unstable intermediate, is formed during the initial stage and transformed into boehmite, eventually. The higher temperature (200 °C) was more energetically favorable for the formation of $NH_4Al_3(SO_4)_2(OH)_6$, and the crystallinity of the products was better. More importantly, the sheet-like structure of boehmite (AlOOH) could be formed at 150 °C after 24 h of reaction time. The SEM results proved that the sheet-like structures evolutionary process of boehmite.

Keywords: alumina hydrate; boehmite; ammonioalunite; evolutionary process; reaction crystallization

1. Introduction

Alumina (Al_2O_3), one of the most important powder materials obtained from calcined alumina hydrates, has been applied in various fields such as in the development of heat-resistant, abrasion-resistant, and corrosion-resistant materials [1,2]. The microscopic morphology of alumina powder is the same as one of its precursors, alumina hydrate [3]. Therefore, it is also necessary to research the synthesis of alumina hydrate. As an important alumina hydrate, boehmite is not only a precursor of alumina, but it also has wide applications in the context of catalysis, surfactants, and adsorbents due to its high surface area mesoporous structure [4,5].

It is well known that alumina is mainly extracted from bauxite; however, the shortage of bauxite is a growing problem in China. In recent years, the extraction of alumina from high-alumina coal fly ash (HACFA), which is the solid waste contained in aluminum resources, has stimulated great research interest [6–8]. A new process for alumina extraction was developed using HACFA as follows: (a) aluminum ammonium sulfate solutions containing impurities are firstly acquired via leaching HACFA and by using ammonium hydrogen sulfate solutions; (b) relatively pure solid aluminum ammonium sulfate is obtained via impurity removal by cooling crystallization; and (c) the alumina hydrate is prepared via the reaction of solid aluminum ammonium sulfate with ammonia ($NH_3 \cdot H_2O$). For aluminum resource extraction by leaching HACFA and ammonium hydrogen sulfate solutions, the preparation of alumina hydrate by reactive crystallization is a crucial step for controlling the morphology of alumina [9,10].

Hydrothermal methods can generate high-temperature and high-pressure environments, which can help insoluble or poorly soluble powders to achieve dissolution and recrystallization. The phase transformation and achievement of various microscopic morphologies can also be obtained using hydrothermal methods. Peng et al. [11] discovered that the different phase structures of MnO_2 could be obtained using hydrothermal methods. As it is an important chemical synthesis method, reaction crystallization has been used widely in industrial fields. Moreover, hydrothermal reaction crystallization is a method through which crystallization takes place in hydrothermal reactors, and it allows one to obtain supersaturation via a coordination reaction [12]. Huang et al. [13] found that hierarchically boehmite and urchin-like hollow alumina microspheres with interconnected needle-like building blocks can be synthesized using hydrothermal methods. Therefore, the application of hydrothermal reaction crystallization to solid $NH_4Al(SO_4)_2 \cdot 12H_2O$ and $NH_3 \cdot H_2O$ as a new process for extracting alumina from HACFA could lead to new findings.

Regarding the crystalline structure of alumina hydrate, there are two major categories: $Al(OH)_3$ (gibbsite and bayerite) and $AlOOH$ (diaspore and boehmite) [14]. The preparation of alumina hydrate plays a decisive role in determining the quality and properties of Al_2O_3. The microscopic morphology of the alumina powder inherits the morphology of its precursor, aluminum hydroxide powder, due to the topological conversion between aluminum hydroxide and alumina. For the reaction crystallization between solid $NH_4Al(SO_4)_2 \cdot 12H_2O$ and $NH_3 \cdot H_2O$, Ji et al. [15] revealed that pseudoboehmite was obtained through the reaction crystallization of a solution of ammonium aluminum sulfate $[NH_4Al(SO_4)_2$ (aq)] and ammonia water $[NH_3 \cdot H_2O$ (aq)]. Compared with liquid–liquid reactions, solid–liquid reactions represent a more energy-efficient option. In the liquid–liquid reaction, the solid $NH_4Al(SO_4)_2 \cdot 12H_2O$ was first dissolved into a solution system and then reacted with ammonia to produce alumina hydrate.

In this paper, we focused on the reaction crystallization process between the solid $NH_4Al(SO_4)_2 \cdot 12H_2O$ and $NH_3 \cdot H_2O$. A thermodynamic analysis was used to assess the feasibility of the reaction product at 120–200 °C. The samples were prepared at 150 °C and 200 °C with different reaction times. The phases of the samples were prepared at 150 °C and 200 °C, and the processes that led to the transformation to alumina hydrate and ammonioalunite products were investigated. Additionally, the morphology of the samples obtained at different reaction times was studied, and the evolution process that led to the creation of sheet-like boehmite structures was also investigated.

2. Experimental Section

2.1. Chemicals and Materials

$NH_4Al(SO_4)_2 \cdot 12H_2O$ and $NH_3 \cdot H_2O$ were purchased from Tianjin Zhiyuan Chemical Reagent Co. LTD. (Tianjin, China)

2.2. Sample Preparation

In the hydrothermal (HT) synthesis process, 40 mL of 2.5% $NH_3 \cdot H_2O$ solution and 5 g of solid $NH_4Al(SO_4)_2 \cdot 12H_2O$ were added to a Teflon-lined stainless steel autoclave and kept at different temperatures (150 °C and 200 °C) for a certain time. The samples were collected by centrifugation and washed with distilled water several times. The samples were named as "HT- temperature-time" (e.g., HT-150-24 h means that the sample was kept at 150 °C for 24 h).

2.3. Sample Characterization

X-ray diffraction (XRD) patterns were performed using a Rigaku SmartLab SE diffractometer equipped with a Cu Kα X-ray source and a 2θ range of 10°–80° with 5°/min. The morphology of the sample was monitored using a scanning electron microscope (SEM, TESCAN MIRA LMS). The surface areas and pore volumes of the samples were evaluated by nitrogen physisorption using a surface area and pore size analyzer (Gold APP Instruments V-Sorb 2008P, Beijing, China). The surface areas were estimated using the BET

(Brunauer−Emmett−Teller) method and the pore volumes were determined by the BJH (Barrett−Joyner−Halenda) method.

3. Thermodynamic Analysis

In the standard state, the Van't Hoff formula used was as follows [16]:

$$\Delta G = \Delta G^0 + RT\ln J \tag{1}$$

where ΔG^0 is the Gibbs free energy change at the same temperature and standard pressure, R is the gas constant ($8.3145 \ J \cdot K^{-1} \cdot mol^{-1}$), T is the thermodynamic temperature (K), and J is the entropy in either reaction state.

When the reaction is in equilibrium, i.e., $\Delta G^0 = 0$, J is the equilibrium constant K (m/M) [17]:

$$\Delta G_T^0 = -RT\ln K \tag{2}$$

The Gibbs equation of the reaction in the standard state is as follows [18]:

$$\Delta G = \Delta H - T\Delta S \tag{3}$$

where ΔH is the enthalpy change in the standard state and ΔS is the entropy change in the standard state.

The reactions between the $NH_4Al(SO_4)_2 \cdot 12H_2O$ and $NH_3 \cdot H_2O$ solutions that may have occurred are as follows:

$$NH_4Al(SO_4)_2 + 3NH_3 \cdot H_2O = AlOOH \ (boehmite) + 2(NH_4)_2SO_4 + H_2O \tag{4}$$

$$NH_4Al(SO_4)_2 + 3NH_3 \cdot H_2O = AlOOH \ (diaspore) + 2(NH_4)_2SO_4 + H_2O \tag{5}$$

$$NH_4Al(SO_4)_2 + 3NH_3 \cdot H_2O = Al(OH)_3 \ (gibbsite) + (NH_4)_2SO4 \tag{6}$$

$$NH_4Al(SO_4)_2 + 3NH_3 \cdot H_2O = Al(OH)_3 \ (bayerite) + (NH_4)_2SO4 \tag{7}$$
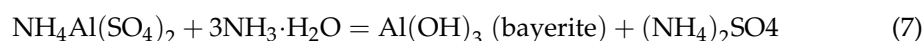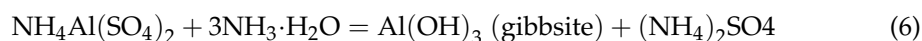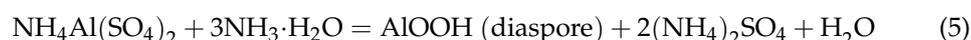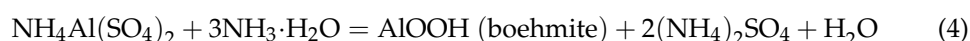
In the reaction crystallization between $NH_4Al(SO_4)_2 \cdot 12H_2O$ and $NH_3 \cdot H_2O$, the $NH_4Al(SO_4)_2 \cdot 12H_2O$ solid is first dissolved into a solution system. Next, hydroxide is obtained by the Al^{3+} combining with the OH^-. Due to the reaction crystallization that took place in the alkaline environment, the OH^- could be effectively disassociated from the $NH_3 \cdot H_2O$ solution. Neither NH_4^+ nor SO_4^{2-} is involved in the main chemical reaction, and the reaction of Equations (4)–(7) can be written as follows:

$$Al^{3+} + 3OH^- = AlOOH(boehmite) + H_2O \tag{8}$$

$$Al^{3+} + 3OH^- = AlOOH(diaspore) + H_2O \tag{9}$$

$$Al^{3+} + 3OH^- = Al(OH)_3 \ (gibbsite) \tag{10}$$

$$Al^{3+} + 3OH^- = Al(OH)_3 \ (bayerite) \tag{11}$$
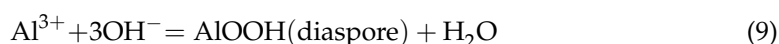
The following products may be produced during reaction crystallization: boehmite, diaspore, gibbsite, and bayerite. However, it is noted that alumina hydrate cannot be formed at a high temperature as reaction (12) may occur and ammonioalunite ($NH_4Al_3(SO_4)_2(OH)_6$) is obtained when NH_4^+, Al^{3+}, and SO_4^{2-} exist simultaneously in the solution [19,20]. However, ammonioalunite is not a common compound. It has rarely been reported and little is known about its chemical and physical characteristics. According to our knowledge, there

are only two papers about ammonioalunite. Wang et al. [20] revealed that an ammonioalunite with a hexagonal rose-like morphology was synthesized via a hydrothermal method at 165 °C, which used $Al_2(SO_4)_3 \cdot 18H_2O$ and urea as the raw materials and cetyltrimethylammonium bromide (CTAB) as the additive. Yang et al. [19] found that ammonioalunite can be obtained, via the hydrothermal synthesis method, in an ammonium aluminum sulfate solution without other raw materials at temperatures of over 180 °C. Additionally, the morphology of ammonioalunite is constituted by irregular particles. If reaction (12) happens in a reaction crystallization system between $NH_4Al(SO_4)_2 \cdot 12H_2O$ and $NH_3 \cdot H_2O$, it will be the first time that ammonioalunite has been synthesized in the alkaline initial environment.

$$NH_4^+ + 3Al^{3+} + 2SO_4^{2-} + 6OH^- = NH_4Al_3(SO_4)_2(OH)_6 \tag{12}$$

In summary, it can be seen that there is a complexity to the reaction crystallization of alumina hydrate. In order to judge the reaction between $NH_4Al(SO_4)_2 \cdot 12H_2O$ and $NH_3 \cdot H_2O$, thermodynamic analysis can be used as the first effective method; furthermore, the important thermodynamic parameters should be calculated, including ΔG, ΔH, and ΔS. These parameter values for the formation of alumina hydrate from $NH_4Al(SO_4)_2 \cdot 12H_2O$ and $NH_3 \cdot H_2O$ at 120 °C, 150 °C, 180 °C, and 200 °C were calculated and are summarized in Table 1. It could be summarized that ΔG_T^0 in reactions (8)–(11) was negative at 120–200 °C; this indicates that these reactions were thermodynamically feasible and spontaneous in nature and that the values did not differ much at the same temperature [21]. In addition, the value of ΔG_T^0 for reactions (8)–(11) decreased with an increase in temperature. Additionally, the increased temperature could contribute to the appropriate formation of alumina hydrate. At 120 °C, the order of the ΔG_T^0 value was as follows: reaction (11) > reaction (8) > reaction (10) > reaction (9). At 200 °C, the order of the ΔG_T^0 value became as follows: reaction (11) > reaction (10) > reaction (8) > reaction (9).

Table 1. Thermodynamic calculations of reactions (8)–(11).

	T/°C	ΔH /(KJ/mol)	ΔS/(J/K)	ΔG /(KJ/mol)	K	Log(K)
Reaction (8)	120	3.188	151.956	−56.554	2.757×10^{31}	31.441
	150	8.558	165.101	−61.305	4.628×10^{31}	31.665
	180	15.431	180.77	−66.485	1.169×10^{32}	32.068
	200	21.146	193.103	−70.221	2.742×10^{32}	32.438
Reaction (9)	120	−1.001	148.645	−59.444	1.116×10^{33}	33.048
	150	4.314	161.664	−64.094	1.277×10^{33}	33.106
	180	11.132	177.207	−69.170	2.305×10^{33}	33.363
	200	16.81	189.461	−72.834	4.414×10^{33}	33.645
Reaction (10)	120	1.246	138.819	−53.330	4.452×10^{29}	29.649
	150	6.464	151.589	−57.681	6.221×10^{29}	29.794
	180	13.218	166.987	−62.452	1.326×10^{29}	30.123
	200	18.87	179.185	−65.911	2.799×10^{29}	30.447
Reaction (11)	120	−2.841	138.507	−57.295	7.123×10^{31}	31.853
	150	2.361	151.24	−61.636	6.864×10^{31}	31.837
	180	9.096	166.592	−66.396	1.058×10^{32}	32.025
	200	14.733	178.757	−69.846	1.841×10^{32}	32.265

For the synthesis of $NH_4Al(SO_4)_2(OH)_6$ in the H_2O system, containing NH_4^+, Al^{3+}, and SO_4^{2-}, the related thermodynamic calculations were conducted by Yang [19], and the relationships between ΔG_T^0 and T in reaction (13) were explored. The results showed that a hydrothermal reaction condition of over 177 °C was required to obtain $NH_4Al_3(SO_4)_2(OH)_6$. Reaction (12) was similar to reaction (13), while the only different reactant was OH^- in

reaction (12) when compared with H_2O in reaction (13). Therefore, the values of ΔG_T^0 are close together and similar.

$$NH_4^+ + 3Al^{3+} + 2SO_4^{2-} + 6H_2O = NH_4Al_3(SO_4)_2(OH)_6 + 6H^+ \tag{13}$$

The negative ΔH for reactions (9) and (11) at 120–200 °C indicated that the reactions were exothermic, while the rest of the ΔH values were positive, which indicated that the reactions were endothermic [22]. The positive ΔS values suggested a degree of disorder in the system and ΔS increased with temperature; thus, the degree of disorder in the reaction system increased [23]. Additionally, all the theoretical possibilities and the feasibility of these reactions were illustrated by thermodynamic calculations, but the actual products could not be determined by thermodynamic data, requiring further investigation.

Previous work by our group indicated that boehmite would be produced by reaction crystallization between $NH_4Al(SO_4)_2 \cdot 12H_2O$ and $NH_3 \cdot H_2O$ in a low-temperature and atmospheric pressure environment [24]. As one of the effective methods for controlling product morphology and phases, the change in hydrothermal temperature should be focused on. In this study, 150 °C and 200 °C were selected as the research temperatures, considering the reasons for forming the condition of $NH_4Al_3(SO_4)_2(OH)_6$.

4. Results and Discussion

4.1. XRD Analysis

To determine the phase structure of the reactant and products, XRD analysis was used, and the patterns are presented in Figures 1–3. As is shown in Figure 1, the XRD patterns of the $NH_4Al(SO_4)_2 \cdot 12H_2O$ (starting solid) reactant corresponded with the standard XRD pattern (PDF No. 71-2203).
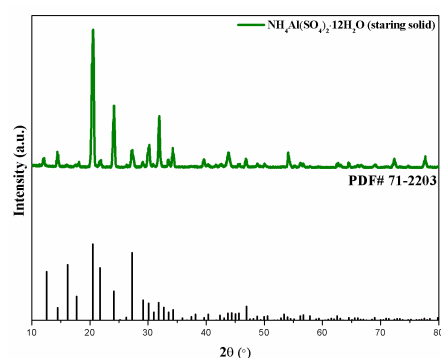
Figure 1. XRD patterns of $NH_4Al(SO_4)_2 \cdot 12H_2O$ (starting solid).

(a)　　　　　　　　　　　　　　　　　　(b)
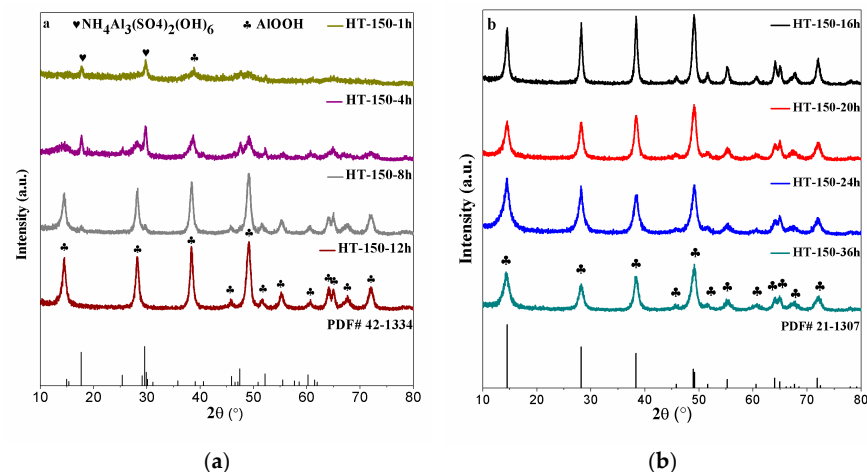
Figure 2. XRD patterns of samples at 150 °C. (**a**) HT-150-1 h, HT-150-4 h, HT-150-8 h, and HT-150-12 h samples, and (**b**) HT-150-16 h, HT-150-20 h, HT-150-24 h, and HT-150-36 h samples.
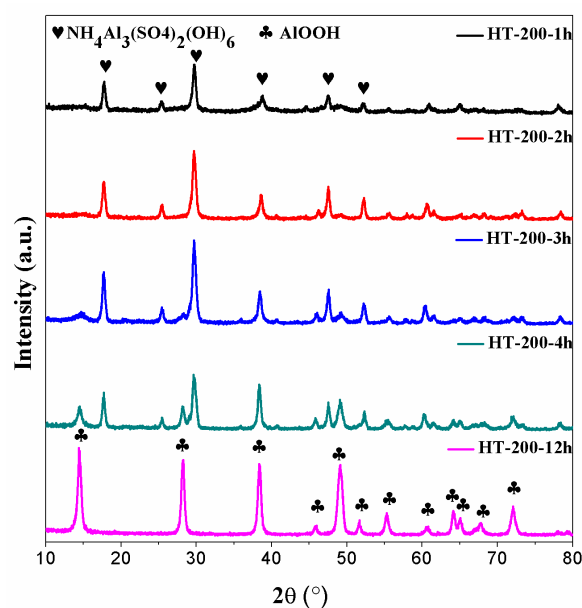
Figure 3. XRD patterns of samples at 200 °C.

The XRD patterns of the hydrothermal samples at 150 °C with different reaction times (1 h, 4 h, 8 h, 12 h, 16 h, 20 h, 24 h, and 36 h) are shown in Figure 2. For the HT-150-1 h sample, only three small peaks at 17.6°, 29.5°, and 38.8° could be observed. The peaks at 17.6° and 29.5° were associated with $NH_4Al_3(SO_4)_2(OH)_6$ (PDF No. 42-1334) [19], and the peak at 38.8° was attributed to the characteristic peaks of boehmite (AlOOH) [6]. This indicated that the crystallized product was formed after 1 h with the fundamental amorphous phase. Additionally, there were no obvious diffraction peaks that could be observed; thus, the phase of the HT-150-1 h sample could not be accurately determined. For the HT-150-4 h sample, diffraction peaks at 17.6° and 29.5° could also be observed, and other diffraction peaks with smaller intensities and broader widths could be observed at 14.5°, 28.1°, 38.3°, 48.8°, 51.5°, 55.1°, 60.5°, 63.8°, 64.8°, 67.5°, and 72.1°, which were associated with the crystal structure of boehmite. This indicated that the phase of boehmite formed gradually in the HT-150-4 h sample. When the reaction time reached eight hours, diffraction peaks corresponding to $NH_4Al_3(SO_4)_2(OH)_6$ were barely observed, except for the small peaks at 17.6° and 29.5°. Additionally, the remaining peaks belonged to boehmite. With the reaction time extended to twelve hours, the peaks of $NH_4Al_3(SO_4)_2(OH)_6$ completely disappeared, and the intensity of the peaks corresponding to boehmite were enhanced, which indicated that good boehmite crystallinity was formed in the HT-150-12 h sample. Between the HT-150-16 h, HT-150-20 h, HT-150-24 h, and HT-150-36 h samples, the XRD patterns showed similar diffraction peaks, as is shown in Figure 2b. All the diffraction peaks corresponding to boehmite (PDF No. 21-1307) were found in the hydrothermal product. Noticeably, diffraction peaks assigned to $NH_4Al_3(SO_4)_2(OH)_6$ were observed in the HT-150-1 h and HT-150-4 h samples at 17.6° and 29.5°, which indicated that a decent amount of $NH_4Al_3(SO_4)_2(OH)_6$ could be formed at 150 °C.

Figure 3 shows the XRD patterns of the hydrothermal samples at 200 °C with different reaction times (1 h, 2 h, 3 h, 4 h, and 12 h). For the HT-200-1 h sample, diffraction peaks around 17.6°, 25.2°, 29.5°, 38.6°, 47.3°, and 51.9° were ascribed to the characteristic reflections of $NH_4Al_3(SO_4)_2(OH)_6$ [19]. This indicated that when the hydrothermal temperature reached 200 °C, the reaction product was not alumina hydrate but $NH_4Al_3(SO_4)_2(OH)_6$. This was also the first time that the synthesis of $NH_4Al_3(SO_4)_2(OH)_6$ occurred under initial alkaline conditions. Noticeably, with prolonged reaction times, the transformation of phases for the hydrothermal sample at 200 °C took place. When the reaction time reached 12 h, the crystallized product was completely transformed into boehmite at a 150 °C reaction temperature. Additionally, the same condition occurred at a 200 °C hydrothermal

temperature, where no $NH_4Al_3(SO_4)_2(OH)_6$ peak could be observed in the HT-200-12 h sample and diffraction peaks of boehmite with a good crystallinity were observed.

The XRD data indicated that the reaction product was boehmite, transformed from $NH_4Al(SO_4)_2(OH)_6$ with the increase in reaction time, which occurred regardless of whether the hydrothermal temperature was 150 °C or 200 °C. Therefore, $NH_4Al_3(SO_4)_2(OH)_6$ is an unstable intermediate. Combined with the results of Figures 1–3, the solid phase transition that took place in this reaction system was as follows: $NH_4Al(SO_4)_2 \cdot 12H_2O \rightarrow NH_4Al_3(SO_4)_2(OH)_6 \rightarrow AlOOH$. In addition, the generation of $NH_4Al(SO_4)_2 \cdot 12H_2O$ in the initial phase when the temperature increased from 150 °C to 200 °C was favored. Moreover, the crystallinity of the product (for both $NH_4Al(SO_4)_2 \cdot 12H_2O$ and AlOOH) was also beneficial.

For this solution system—which contained NH_4^+, Al^{3+}, SO_4^{2-}, and OH^- simultaneously—the formation of alumina hydrate or $NH_4Al_3(SO_4)_2(OH)_6$ has been previously reported; however, the transformations of these compounds have yet to be reported. It has been reported that rose-like ammonioalunite produced from $Al_2(SO_4)_3 \cdot 18H_2O$ and urea, with cetyltrimethylammonium bromide (CTAB) as the additive, is produced via the hydrothermal method at 165 °C and 4 h [20]. Nevertheless, boehmite (γ-AlOOH) hollow microspheres were synthesized from $Al_2(SO_4)_3 \cdot 18H_2O$ and urea, and the production of the amphiphilic block copolymer of poly-styrene-block-poly-hydroxyl-ethyl acrylate (PS-b-PHEA), as a structure-directing reagent, via hydrothermal synthesis at 150 °C and 24 h was also achieved [25]. In the two studies mentioned above, different products—$(NH_4Al_3(SO_4)_2(OH)_6$ and γ-AlOOH)—could be obtained from the same reactants $(Al_2(SO_4)_3 \cdot 18H_2O$ and urea) at a similar temperature. It is well known that the phase of the product is not affected by the template. Thus, this reflects the complicated nature of a solution system that contains NH_4^+, Al^{3+}, SO_4^{2-}, and OH^- simultaneously. Significantly, it could be found that the synthesis time for $NH_4Al(SO_4)_2(OH)_6$ is lower than alumina hydrate, and that the synthesis time is relatively long for alumina hydrate when using the hydrothermal method. This was also consistent with our experimental results, although aluminum ammonium sulfate $(NH_4Al(SO_4)_2 \cdot 12H_2O)$ was used as an aluminum source in our experiment. In addition, we have reason to believe that alumina hydrate with a specific morphology can be obtained as the reaction is extended.

$NH_4Al_3(SO_4)_2(OH)_6$ has potential application value in the fields of artificial gemstones, catalyst carriers, sewage treatment, corundum products, etc. [20,26]. However, alumina hydrate from CFA is a better choice for recycled aluminum resources because it is more energy efficient when compared to ammonioalunite. It is the most widespread and in demand application, as is the preparation of aluminum (Al) through the electrolytic reduction of alumina (Al_2O_3) and as Al_2O_3 is from the calcination of alumina hydrate. More synthetic paths would provide a more certain basis for its application, and the synthesis of it from CFA would provide a much greater variety.

4.2. SEM Analysis

Figure 4 shows the morphology of the HT-150-24 h sample. A large amount of the sheet-like structure, with distinguishable boundaries of boehmite (AlOOH), was observed in the HT-150-24 h sample. Additionally, the rose-like structures were composed of nanosheet building blocks, which were also unstable. It was reported that boehmite crystals prefer to grow into nano-flakes under weak, basic hydrothermal conditions, owing to their distinctly AlO_6-octahedral-layered structure, which possesses a great deal of surface-located OH-groups [27,28]. The boehmite samples in the literature exhibit mainly flake-like structures that have a length of approximately 600 nm and a width of around 250 nm [28]. In our research, the boehmite sample exhibited mainly sheet-like morphologies with a length of around 1.6 μm and a width of approximately 0.5 μm. In order to investigate the evolutionary process of the sheet-like structure of the AlOOH crystals, SEM was performed on the whole samples at a hydrothermal temperature of 150 °C. Several representative pictures of this process are shown in Figure 5.
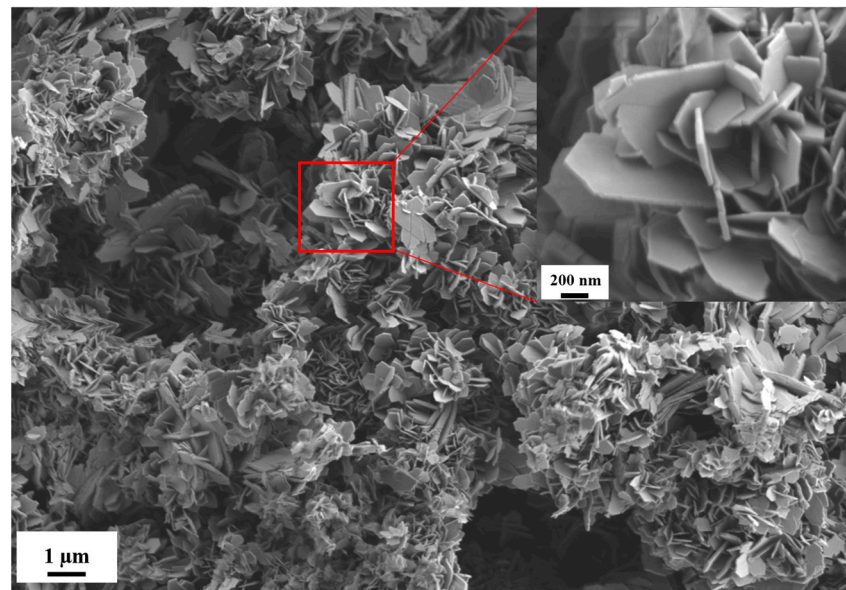
Figure 4. SEM images of the HT-150-24 h sample.
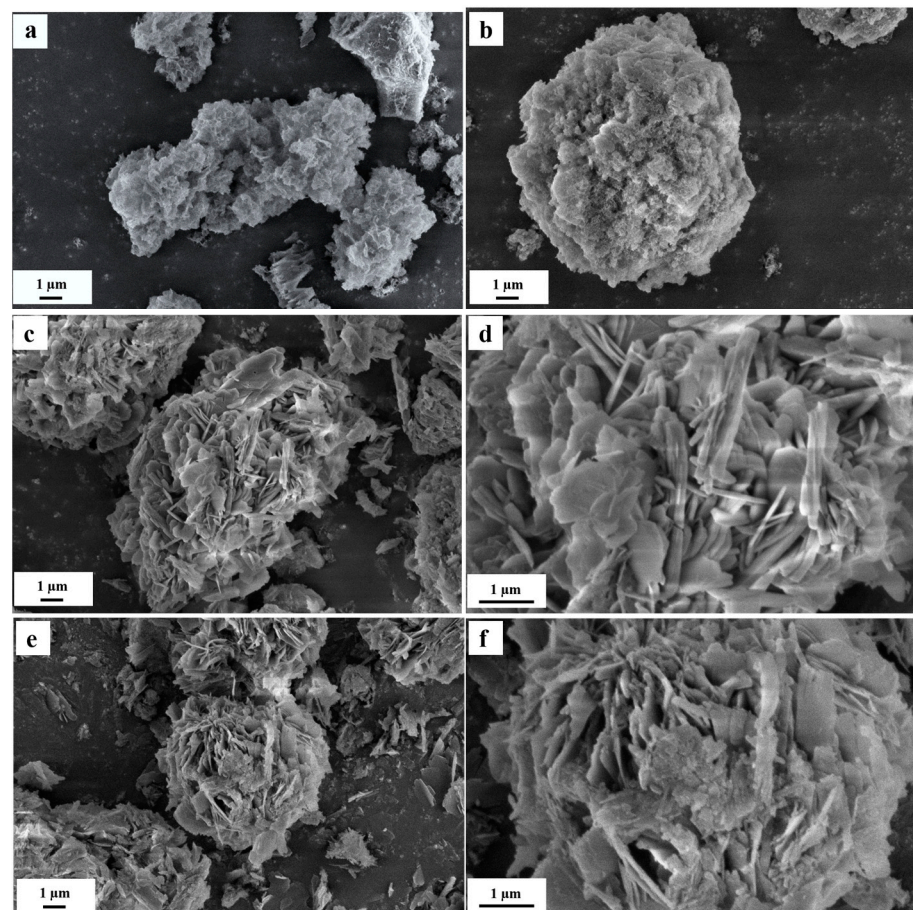
Figure 5. SEM images of the different samples. (**a**): HT-150-1 h; (**b**): HT-150-4 h; (**c**,**d**): HT-150-8 h; and (**e**,**f**): HT-150-20 h.

As is shown in Figure 5, structures of irregular morphology with coarse and loose surfaces appeared in the HT-150-1 h and HT-150-4 h samples. These samples had a certain pore-like structure, and the integrated granules could hardly be observed in the HT-150-1 h sample. In the beginning of the reactive crystallization process, along with the gradual

hydrolysis of $NH_4Al(SO_4)_2 \cdot 12H_2O$, Al^{3+} and SO_4^{2-} began to increase substantially, and $NH_4Al_3(SO_4)_2(OH)_6$ might thus be formed. Combined with the XRD results, certain $NH_4Al_3(SO_4)_2(OH)_6$ crystals were formed in the HT-150-1 h and HT-150-4 h samples. According to the reported literature, amorphous phase clusters form in the initial stage of the hydrothermal reaction; furthermore, the amorphous phase is unstable due to its higher solubility [29]. Additionally, its dissolved–recrystallized process and slow-phase transformation could have occurred in the amorphous phase as a more thermodynamically stable product could be obtained step by step. It can be inferred that boehmite is a more thermodynamically stable crystal when compared with $NH_4Al_3(SO_4)_2(OH)_6$. In the HT-150-8 h sample, particles with lamellar- and strip-like structures can be simultaneously observed. Additionally, as the reaction progressed in the HT-150-20 h sample, the strip-like structure disappeared, and the particle with an extensive lamellar-like structure was formed. On the basis of the XRD results, boehmite was completely formed in the HT-150-12 h sample without $NH_4Al_3(SO_4)_2(OH)_6$. Therefore, it could be suggested that the lamellar-like structure of the particle shown in Figure 6e is boehmite. When the reaction time reached 24 h, it was presumed that the sheet-like structure of boehmite appeared through a partial dissolution of particles with a lamellar-like structure. In conclusion, the morphology's evolutionary process of boehmite was as follows: amorphous phase clusters → particles with lamellar-like and strip-like structures → particles with more lamellar-like structures → sheet-like structures. Additionally, as the reaction time continued to extend, no regular and special morphologies could be observed in the HT-150-36 h sample.
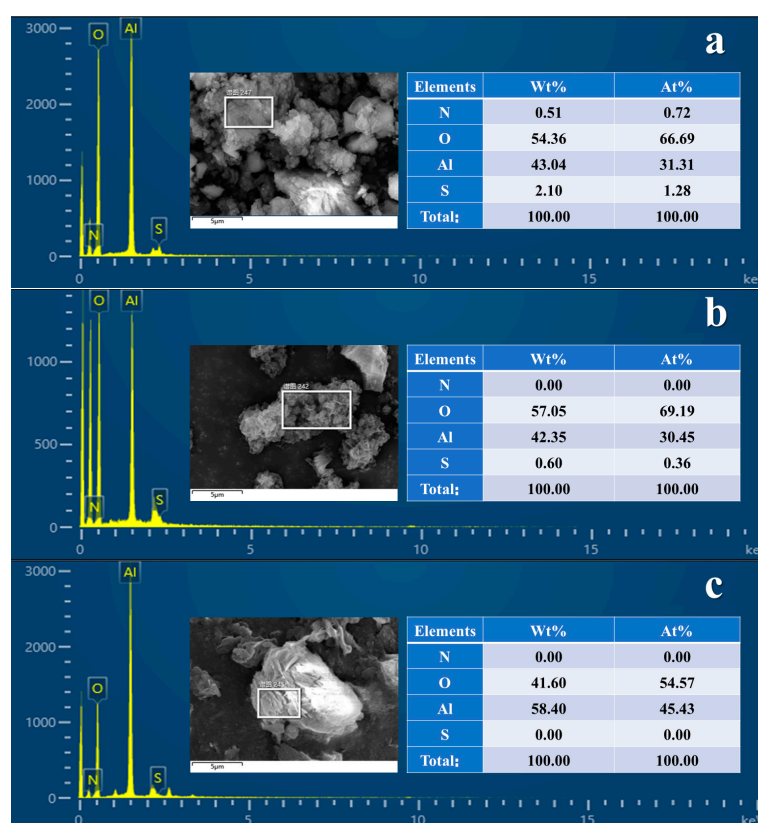
Figure 6. The energy spectra of the samples. (**a**): HT-150-1 h; (**b**): HT-150-4 h; and (**c**): HT-150-16 h.

4.3. Energy Spectrum Analysis

The energy spectra of the HT-150-1 h, HT-150-4 h, and HT-150-16 h samples are presented in Figure 6. For the HT-150-1 h sample, the element wt% values of N, O, Al, and S were 0.51%, 54.36%, 43.04%, and 2.10%, respectively. It was confirmed that the minor quantities of the S and N elements were present in the HT-150-1 h sample, which further validated the little $NH_4Al_3(SO_4)_2(OH)_6$ crystals that formed in the HT-150-1 h sample. As

the reaction progressed, the element wt% values of the N and S in the HT-150-16 h sample decreased gradually until they reached 0. Furthermore, the element wt% values of the O and Al were 41.60% and 58.4%, respectively. These findings were fully consistent with the XRD results.

4.4. BET Analysis

Figure 7 shows the N_2 absorption–desorption isotherm and the pore-size distribution of the HT-150-16 h, HT-150-20 h, and HT-150-24 h samples. All the samples showed type IV isotherms, according to the BDDT classification, which implies that all the three samples belong to mesoporous materials. The isotherms of the three samples exhibited a typical H3 hysteresis loop as the closure points existed at a low P/P_0 ($P/P_0 = 0.45$). The BJH desorption pore-size distributions that were evaluated from the N_2 desorption isotherm are presented in Figure 7b. It was evident that the desorption pore-size distributions of the three catalysts gathered at 10–100 nm. The HT-150-16 h and HT-150-20 h samples showed a wider distribution peak, which indicated that the HT-150-16 h and HT-150-20 h samples had a more abundant mesoporous structure when compared with the HT-150-24 h sample.
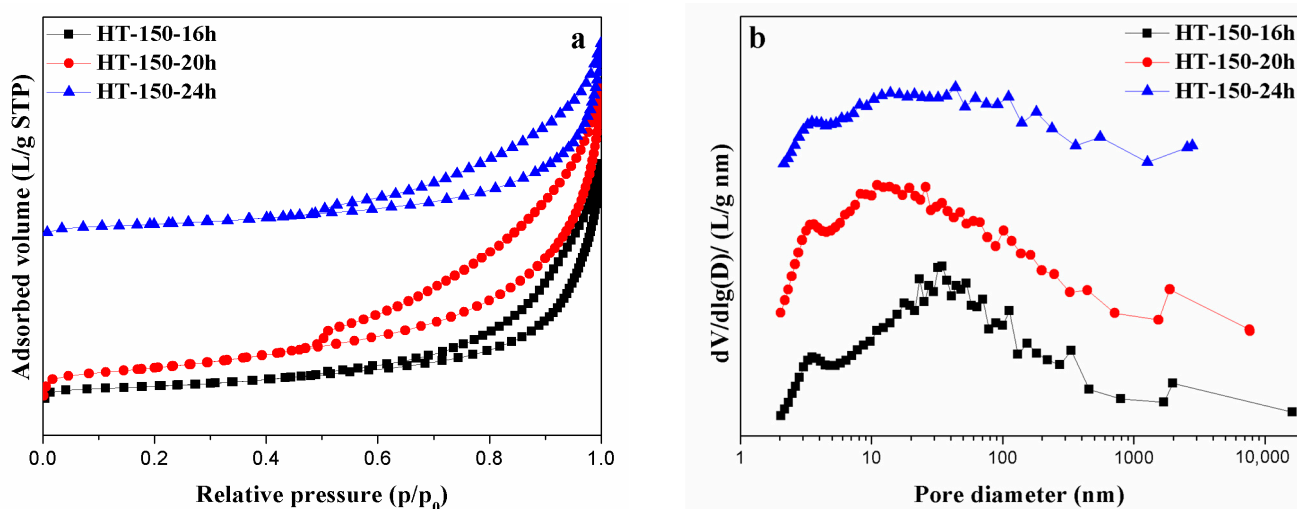
Figure 7. N_2 absorption–desorption results of the HT-150-16 h, HT-150-20 h, and HT-150-24 h samples. (**a**) N_2 absorption–desorption isotherm; and (**b**) pore-size distributions.

Table 2 lists the BET surface areas, pore volumes, and average pore size of the HT-150-16 h, HT-150-20 h, and HT-150-24 h samples. It can be seen that the HT-150-20 h sample possesses the largest specific surface area (88.317 m^2/g) and pore volume (0.344 cm^3/g). The specific surface area and pore volume were greater when compared with the HT-150-16 h sample. However, the BET surface areas, pore volume, and average pore size of the HT-150-24 h sample were 41.573 m^2/g, 0.212 cm^3/g, and 15.257 nm, respectively. This represented the smallest value among the three samples. Combined with the results of the SEM analysis, when the reaction time of 16 h was increased to 20 h, the specific surface area and pore volume were increased due to more lamellar-like structures appearing and the strip-like structure disappearing. Additionally, when the reaction time increased to 24 h, the particles with a great number of lamellar-like structures dissolved into sheet-like structures. The specific surface area decreased to 46.744 m^2/g and the pore volume decreased to 0.132 cm^3/g. The BET results provided supporting evidence for the process of the sheet-like-structured boehmite.

Table 2. Structural parameters of the samples.

Samples	S_{BET} (m^2/g)	Pore Volume (cm^3/g)	Average Pore Size (nm)
HT-150-16 h	45.110	0.258	17.939
HT-150-20 h	88.317	0.344	12.309
HT-150-24 h	41.573	0.212	15.257

5. Conclusions

For the hydrothermal reaction crystallization process between a $NH_4Al(SO_4)_2 \cdot 12H_2O$ solid and $NH_3 \cdot H_2O$, the thermodynamic analysis indicated that all four kinds of alumina hydrate (boehmite, diaspore, gibbsite, and bayerite) might be formed. The experimental and characterization results showed that boehmite (AlOOH) was formed at 150 °C and 200 °C after a 12 h reaction. Additionally, $NH_4Al_3(SO_4)_2(OH)_6$ was found to be an unstable intermediate; however, it did eventually transform into boehmite. This study represents the first time that $NH_4Al_3(SO_4)_2(OH)_6$ has been prepared under initial alkaline conditions. The higher temperature (200 °C) was more energetically favorable for the formation of $NH_4Al_3(SO_4)_2(OH)_6$, and the crystallinity of the products (both $NH_4Al_3(SO_4)_2(OH)_6$ and AlOOH) could be improved. Most importantly, however, it was found that the sheet-like structure of boehmite (AlOOH) can be formed at 150 °C and in 24 h. The SEM results prove the evolutionary process of boehmite with a sheet-like-structure.

Institutional Review Board Statement: "Not applicable" for studies not involving humans or animals.

Data Availability Statement: The data underlying the results presented in this paper are not publicly available at this time but may be obtained from the authors upon reasonable request.

Conflicts of Interest: We have no relevant financial interests to disclose. None of the authors have any financial or scientific conflicts of interest with respect to the research described in this manuscript.

References

1. Zhang, W.; Wang, S.; Zhao, L.; Ran, J.; Kang, W.; Feng, C.; Zhu, J. Investigation of Low-Calcium Circulating Fluidized Bed Fly Ash on the Mechanical Strength and Microstructure of Cement-Based Material. *Crystals* **2022**, *12*, 400. [CrossRef]
2. Luțcanu, M.; Cimpoeșu, R.; Abrudeanu, M.; Munteanu, C.; Moga, S.G.; Coteata, M.; Zegan, G.; Benchea, M.; Cimpoeșu, N.; Murariu, A.M. Mechanical Properties and Thermal Shock Behavior of Al_2O_3-YSZ Ceramic Layers Obtained by Atmospheric Plasma Spraying. *Crystals* **2023**, *13*, 614. [CrossRef]
3. Frazer, I.H.; Leggatt, G.R.; Mattarollo, S.R. Prevention and treatment of papillomavirus-related cancers through immunization. *Annu. Rev. Immunol.* **2011**, *29*, 111–138. [CrossRef] [PubMed]
4. Chen, S.; Yang, S.; Cheung, C.F.; Liu, T.; Duan, D.; Ho, L.-T.; Jiang, Z. Study on the Surface Generation Mechanism during Ultra-Precision Parallel Grinding of SiC Ceramics. *Crystals* **2023**, *13*, 646. [CrossRef]
5. Vo, D.D.; Alsarraf, J.; Moradikazerouni, A.; Afrand, M.; Salehipour, H.; Qi, C. Numerical investigation of γ -AlOOH nano-fluid convection performance in a wavy channel considering various shapes of nanoadditives. *Powder Technol.* **2019**, *345*, 649–657. [CrossRef]
6. Wu, Y.S.; Xu, P.; Li, L.S. Synthesis of alumina with coarse particle by precipitating aluminum ammonium sulfate solution with ammonia. *Adv. Powder Technol.* **2016**, *27*, 124–129. [CrossRef]
7. Alterary, S.S.; Marei, N.H. Fly ash properties, characterization, and applications: A review. *J. King Saud Univ. Sci.* **2021**, *33*, 101536. [CrossRef]
8. Ma, Y.; Stopic, S.; Xakalashe, B.; Ndlovu, S.; Forsberg, K.; Friedrich, B. A cleaner approach for recovering Al and Ti from coal fly ash via microwave assisted baking, leaching and precipitation. *Hydrometallurgy* **2021**, *206*, 105754. [CrossRef]

9.   Yang, X.; Wu, Y.; Li, L.; Wang, Y.; Li, M. Crystallization mechanism of ammonium aluminum sulfate during cooling process. *J. Cryst. Growth* **2021**, *560–561*, 126064. [CrossRef]

10. Wu, Y.; Yang, X.; Li, L.; Wang, Y.; Li, M. Kinetics of extracting alumina by leaching coal fly ash with ammonium hydrogen sulfate solution. *Chem. Pap.* **2019**, *73*, 2289–2295. [CrossRef]

11. Peng, Y.; Chang, H.; Dai, Y.; Li, J. Structural and surface effect of MnO$_2$ for low temperature selective catalytic reduction of NO with NH$_3$. *Procedia Environ. Sci.* **2013**, *18*, 384–390. [CrossRef]

12. Wang, F.; Zhu, L.; Wei, Q.; Wang, Y. Research on the effects of hydrothermal synthesis conditions on the crystal habit of MIL-121. *R. Soc. Open Sci.* **2020**, *7*, 201212. [CrossRef] [PubMed]

13. Huang, H.; Wang, L.; Cai, Y.; Zhou, C.; Yuan, Y.; Zhang, X.; Wan, H.; Guan, G. Facile fabrication of urchin-like hollow boehmite and alumina microspheres with a hierarchical structure via Triton X-100 assisted hydrothermal synthesis. *CrystEngComm* **2015**, *17*, 1318–1325. [CrossRef]

14. Kloprogge, J.T.; Duong, L.V.; Wood, B.J.; Frost, R.L. Xps study of the major minerals in bauxite: Gibbsite, bayerite and (pseudo-)boehmite. *J. Colloid Interface* **2006**, *296*, 572–576. [CrossRef]

15. Ji, Y.; Wu, Y.; Li, L. Synthesis and characterization of pseudoboehmite by neutralization method. *Ceram. Int.* **2021**, *47*, 15923–15930. [CrossRef]

16. Ahsendorf, T.; Wong, F.; Eils, R.; Gunawardena, J. A framework for modelling gene regulation which accommodates non-equilibrium mechanisms. *BMC Biol.* **2014**, *12*, 102. [CrossRef]

17. Teng, Y.; Liu, Z.; Yao, K.; Song, W.; Sun, Y.; Wang, H.; Xu, Y. Preparation of Attapulgite/CoFe$_2$O$_4$ magnetic composites for efficient adsorption of tannic acid from aqueous solution. *Int. J. Environ. Res. Public Health* **2019**, *16*, 2187. [CrossRef]

18. Xie, F.; Zhang, J.; Chen, J.; Wang, J.; Wu, L. Research on enrichment of P$_2$O$_5$ from low-grade carbonaceous phosphate ore via organic acid solution. *J. Anal. Method Chem.* **2019**, *3*, 1–7. [CrossRef]

19. Yang, X.; Wu, Y.; Li, L.; Wang, Y.; Li, M. Thermodynamics of ammonioalunite precipitation in ammonium aluminum sulfate solution. *Hydrometallurgy* **2020**, *195*, 105393. [CrossRef]

20. Wang, F.; Zhu, J.; Liu, H. Hydrothermal Synthesis of Ammonioalunite with Hexagonal Rose-like Morphology. *Mater. Lett.* **2018**, *216*, 269–272. [CrossRef]

21. Ueoka, N.; Oku, T. Stability Characterization of PbI$_2$-Added CH$_3$NH$_3$PbI$_{3-x}$Cl$_x$ Photovoltaic Devices. *ACS Appl. Mater. Interfaces* **2018**, *51*, 44443–44451. [CrossRef] [PubMed]

22. Lee, J.; Hwang, T.; Cho, H.B.; Kim, J.; Choa, Y.H. Near theoretical ultra-high magnetic performance of rare-earth nanomagnets via the synergetic combination of calcium-reduction and chemoselective dissolution. *Sci. Rep.* **2018**, *8*, 15656. [CrossRef] [PubMed]

23. Liu, J.; Huang, L.; Xie, W.; Kuo, J.; Buyukada, M.; Evrendilek, F. Bioresource Technology Characterizing and optimizing (co-)pyrolysis as a function of different feedstocks, atmospheres, blend ratios, and heating rates. *Bioresour. Technol.* **2019**, *277*, 104–116. [CrossRef] [PubMed]

24. Ma, X.; Wu, Y.; Li, L.; Wang, Y. Effect of SDBS on crystallization behavior of pseudoboehmite. *J. Phys. Chem. C* **2021**, *125*, 26039–26048. [CrossRef]

25. Wu, X.; Wang, D.; Hu, Z.; Gu, G. Synthesis of γ-AlOOH (γ-Al$_2$O$_3$) self-encapsulated and hollow architectures. *Mater. Chem. Phys.* **2008**, *109*, 560–564. [CrossRef]

26. Akar, S.T.; Akar, T.; San, E. Chitosan-alunite composite: An effective dye remover with high sorption, regeneration and application potential. *Carbohydr. Polym.* **2016**, *143*, 318–326. [CrossRef]

27. Zhang, L.; Lu, W.; Cui, R.; Shen, S. One-pot template-free synthesis of mesoporous boehmite core–shell and hollow spheres by a simple solvothermal route. *Mster Res. Bull.* **2010**, *45*, 429–436. [CrossRef]

28. Cai, W.; Yu, J.; Gu, S.; Jaroniec, M. Facile hydrothermal synthesis of hierarchical boehmite: Sulfate-mediated transformation from nanoflakes to hollow microspheres. *Cryst. Growth Des.* **2010**, *10*, 3977–3982. [CrossRef]

29. Wu, X.; Zhang, B.; Wang, D.; Hu, Z. Morphology evolution studies of boehmite hollow microspheres synthesized under hydrothermal conditions. *Mater. Lett.* **2012**, *70*, 128–131. [CrossRef]